Morphology and size of the particles emitted from a GDI-engine vehicle and their ageing in an environmental chamber

Jiaoping Xing[a,b], Longyi Shao[a] *, Wenbin Zhang[c], Jianfei Peng[d], Wenhua Wang [a] , Shijin Shuai[c], Min Hu[d], Daizhou Zhang[e] *

[a]State Key Laboratory of Coal Resources and Safe Mining, School of Geoscience and Survey Engineering, China University of Mining and Technology (Beijing), Beijing 100083, China.
[b]2011 Collaborative Innovation Center of Jiangxi Typical Trees Cultivation and Utilization, School of Forestry, Jiangxi Agricultural University, Nanchang, 330045, China.
[c]State Key Laboratory of Automotive Safety and Energy, Department of Automotive Engineering, Tsinghua University, Beijing 100084, China
[d]State Key Joint Laboratory of Environmental Simulation and Pollution Control, College of Environmental Sciences and Engineering, Peking University, Beijing 100871, China
[e]Faculty of Environmental and Symbiotic Sciences, Prefectural University of Kumamoto, Kumamoto 862-8502, Japan

* Corresponding Author - e-mail: shaoL@cumtb.edu.cn (Longyi Shao); dzzhang@pu-kumamoto.ac.jp (Daizhou Zhang)

Highlights

1. Particles from a GDI-engine vehicle and their ageing were studied.

2. GDI-engine vehicles contribute significantly to both primary and secondary organic particles.

3. Higher contents of organic particles were emitted under hot stabilized running and hot start states.

4. Sulfate and secondary organic aerosol form on the surface of primary particles after ageing.

5. Particles aged rapidly by catalyzed acidification under high pollution levels in Beijing.

Abstract:

Air pollution is particularly severe in developing megacities, such as Beijing, where pollutants from vehicles equipped with modern gasoline direct injection (GDI) engines must be paid enough attention. This study presents the characteristics of individual particles emitted by a GDI gasoline vehicle and their ageing in a smog chamber under the Beijing urban environment, as part of the Atmospheric Pollution & Human Health (APHH) research programme. Using electron microscopy, we identified the particles emitted from a commercial GDI-engine vehicle running under various conditions, namely cold start, hot start, hot stabilized running, idle, and acceleration states. Our results show that most of the particles were organic, soot and Ca-rich ones, with small quantities of S-rich and metal-containing particles. In terms of grain size, the particles exhibited a bimodal distribution in number *vs* size, with one mode at 800–900 nm, and the other at 140–240 nm. The amounts of organic particles emitted under hot start and hot stabilized states were higher than those emitted under other conditions. The amount of soot particles was higher under cold start and acceleration states. Under the idle state, the proportion of Ca-rich particles was highest, although their absolute number was low. In addition to quantifying the types of particles emitted by the engine, we studied the ageing of the particles during 3.5 hours of photochemical oxidation in an environmental chamber under the Beijing urban environment. Ageing transformed soot particles into core-shell structures, coated by secondary organic species, while the content of sulfur in Ca-rich and organic particles increased. Overall, the majority of particles from GDI-engine vehicles are organic and soot particles with submicron or

57   nanometric size. The particles are highly reactive; they react in the atmosphere and

58   change their morphology and composition within hours via catalyzed acidification that

59   involves gaseous pollutants under high pollution levels in Beijing.

60

1. Introduction

62   Air pollution caused by $PM_{2.5}$ in megacities such as Beijing, the capital city of

63   China, is of public and academic concern due to its environmental impacts (Bond et al.

64   2013, Huang et al. 2014, Liu et al. 2017,) and adverse health effects (Chart-asa and

65   Gibson 2015, Shao et al. 2017). PM (particulate matter) emissions from vehicles are

66   one of the most significant sources of airborne particles in the urban atmosphere, and

67   contribute up to 31% of primary particulate emissions of $PM_{2.5}$ in Beijing (Yu et al.

68   2013). Moreover, secondary aerosol formation associated with traffic emissions is a

69   major process leading to the rapid increase of $PM_{2.5}$, which results in severe haze

70   episodes (Huang et al. 2014). Although emissions from gasoline engines are relatively

71   lower than those from diesel engines (Alves et al. 2015), the number of gasoline-

72   powered vehicles in urban areas greatly exceeds that of diesel-powered vehicles. The

73   total number of vehicles in China reached 310 million in 2017, about 70% of these were

74   powered by gasoline engines (National Bureau of Statistics of China, 2018). There are

75   two main types of gasoline engines, namely conventional multipoint port fuel injection

76   (PFI) engines and gasoline direct injection (GDI) engines. In recent years, the demand

77   for engines with high efficiency and low fuel consumption has led to an increasing use

78   of GDI engines in light-duty passenger cars. The market share of GDI-engine vehicles

79   has increased dramatically over the past decade and was estimated to reach 50% of new

80   gasoline vehicles sold in 2016 (Zimmerman et al. 2016). In Beijing and northern China,

81   the vehicle emissions become a more concerned issue in terms of air pollution when

82   the emission from coal combustion are seriously compressed after the Action for

83   Comprehensive Control of Air Pollution in Beijing since 2017 (Chen et al. 2019, Zhang

84   et al. 2019).

85   The number, mass and size distribution of particles emitted from GDI-engine

86   vehicles have been studied (Khalek et al. 2010, Baral et al. 2011, Maricq et al. 2011).

87   The size distribution usually has an accumulation mode with the maxima in the

88   diameter range of 100–300 nm. Major components of the particles include elemental

89   carbon (EC), organic carbon, and ash (Giechaskiel et al. 2014). Besides particulate

90   matter, the engines emit gaseous hydrocarbon compounds. These compounds might

91   form particles, or be adsorbed on the surface of particle aggregates, leading to the

92   growth of the particles in the engine emission (Luo et al. 2015). Relatively high particle

93   emissions by GDI-engine vehicles have prompted studies on the effects of engine

94   operating parameters and fuel composition on the characteristics of the particles (Hedge

95   et al. 2011, Szybist et al. 2011). It has been found that, in general, emissions under the

96   cold start condition make up the major contribution to the total amount of PM emissions

97   from GDI engines (Chen and Stone 2011). Studies have also demonstrated that the

98   highest particle emissions from GDI engines in number concentration occur under the

99   acceleration state during transient vehicle operations (Chen et al. 2017).

100   Studies have also shown that gasoline vehicles are an important source of

101   secondary aerosol precursors in urban areas (Suarez-Bertoa et al. 2015). Secondary

102   aerosols can be formed via gas-phase reactions of volatile organic compounds and

103   multiphase and heterogeneous processes of primary particles (Zhu et al. 2017).

104   Experiments performed in environmental chambers demonstrated that the mass of

105   secondary aerosols derived from precursors could exceed that of directly-emitted

106   aerosols (Jathar et al. 2014). The occurrence of secondary aerosols on particles could

107   change the properties of particles in size, mass, chemical composition, morphology,

108   optical and hygroscopic parameters. These changes, in turn, might affect the

109   environmental impact of the particles significantly, for instance in terms of visibility,

110   human health, weather, and energy budgets (Peng et al. 2017). In general, the ageing

111   processes of primary particles in the atmosphere are studied to understand their climate

112   effects (Niu et al. 2011). However, the lack of data on primary particles emitted by

113   gasoline engines hinders a deep understanding of the roles and activities of the particles

114   in ambient air pollution and relevant environmental effects.

115   APHH-Beijing aimed to explore the sources and processes affecting urban

116   atmospheric pollution in Beijing. Details regarding this project are given in Shi et al.

117   (2018). To address one of the aims of the AIRPOLL-Beijing (Source and Emissions of

118   Air Pollutants) and AIRPRO-Beijing (The integrated Study of AIR Pollution Processes),

119   we employed a dedicated experiment to investigate the characteristics of the individual

120   particles, in terms of the number concentration, size distribution, emitted from a GDI-

121   engine vehicle during a real-world driving cycle for chassis dynamometer test, i.e., the

122   Beijing driving cycle (BDC). Various test modes were introduced to accurately evaluate

123   the emission from light- or medium-duty vehicles. Furthermore, experiments were

124   conducted in an environmental chamber to investigate the ageing processes of particles

125   emitted by GDI-engine vehicles in ambient air in Beijing. We utilized a transmission

126   electron microscope equipped with an Oxford energy-dispersive X-ray spectrometer

127   (TEM-EDX) to identify the morphology, size and elemental composition of particles

128   emitted by the GDI-engine vehicle when it was running under different states. Particles

129   before and after a 3.5-hour ageing in the chamber were compared on the basis of the

130   TEM-EDX analysis. The TEM-EDX analysis could provide the information on the

131   internal inhomogeneity, mixing state and surface characteristics of individual particles

132   and has been used to analyze the aerosol particles (Li and Shao 2009, Adachi and

133   Buseck 2015, Shao et al. 2017). The experimental design allows for the study of the

134   physical and chemical characteristics of the particles emitted from the GDI-engine

135   vehicles, as well as their ageing in a simulated urban atmosphere. The purposes of this

136   study are to evaluate the individual characteristics and the ageing process of primary

137   particles emitted by a GDI-engine vehicle, to investigate the ageing processes of such

138   particles in the atmosphere, and to deepen the understanding of the environmental

139   impact of gasoline-powered vehicle emissions.

140   **2. Material and methods**

141   **2.1 Test vehicle, fuels, and test procedure**

142   The GDI-engine vehicle utilized in the experiment complies with the China Phase

143   4 (equivalent to Euro 4) standard. It uses a three-way catalyst to reduce gaseous

144   emissions. The GDI (model GDI-1.4-T) in the test vehicle is recognized as a

145   representative of leading-edge designs of gasoline engines, having advanced engine

146 technologies, that combine turbocharging and GDI together with a downsized

147 displacement. Vehicles equipped with such GDI engines constitute the majority of light-

148 duty vehicles in China, especially in large cities like Beijing. Details of the engine used

149 in this study are listed in Table S1. The fuel used in the experiment is a commercial

150 gasoline blend of common quality in China. The properties of the fuel were measured

151 by SGS-CSTC Standards Technical Services Co., Ltd., China, and are listed in Table

152 S2. The fuel has a Research Octane Number (RON) of 93 and is a fifth-stage gasoline.

153 It contains, in volume, 36.7% of aromatics and 15.4% of olefins; it also has 6% of sulfur

154 in mass. The experiments were conducted within repeated Beijing driving cycles

155 (BDCs). One BCD included a 200-s "cold start" phase followed by an 867-s "hot

156 stabilized running" phase. The conditions during a BDC in the experiments are

157 illustrated in Figure S1a. The cold start state was achieved by starting the vehicle with

158 a period of small accelerations, while the hot stabilized running state had multiple

159 periods of large acceleration and a maximum velocity of 50 km h^{-1}.

160 All tests were performed on a Euro 5/LEV2/Tier 2-capable test cell on a 48-inch

161 single-roll chassis dynamometer at the State Key Laboratory of Automobile Safety and

162 Energy Conservation at Tsinghua University. The test procedure for each run was as

163 follows: fuel change, BDC preparation, soak, cold start BDC test, and hot start BDC

164 test. After fuel change and BDC preparation, the test vehicle was then conditioned with

165 an overnight soak for more than 10 h. The soak room temperature was maintained

166 between 20 and 30 °C. Due to the limitation of the facilities and available running time,

167 a hot start test was conducted within 5 mins after the cold start test. A dilution unit was

168   applied to dilute the exhaust from the tailpipe into 1/10 in volume using synthetic air

169   composed of 79% N_2 and 20% O_2, in order to obtain the concentrations suitable for

170   subsequent measurements and suppress possible coagulation. The number

171   concentration of the emitted particles was monitored by a Combustion Fast Particle

172   Size Spectrometer Differential Mobility Spectrometer 500 (DMS 500). The maximum

173   measurable number concentration of DMS 500 was 10^{11} (dN/dlogDp/cc) after the

174   dilution (Petzold et al. 2011). For the analyses of individual particles, 6–8 samples were

175   collected during one BDC test. At least one sample was collected under each running

176   state (i.e. cold start, hot start, idle state, acceleration state, or hot stabilized running

177   state). The driving cycle test was repeated at least twice. Two or more samples were

178   obtained for each running state. A single-stage cascade impactor was mounted to the

179   exit of the tailpipe after the dilution unit. The emitted particles were collected onto 300-

180   mesh copper TEM grids, which were covered with a carbon-coated formvar film. The

181   flow rate was 1.0 L min^{-1}, and the cut-off diameter of the impactor for 50% collection

182   efficiency was 0.25 μm if the density of the particles was 2 g cm^{-3}. For each sample, the

183   collection time was 60 s.

184   **2.2 Environmental chamber experiments**

185   Particles from the GDI-engine vehicle were introduced into an environmental

186   chamber and exposed to sunlight. The chamber, made of perfluoroalkoxy (PFA) Teflon

187   in order to achieve a high transmission of ultraviolet light, had an internal volume of

188   1.2 m^3. Ambient sunlight was used as the driving force for photochemical reactions in

189   the chamber, in an environment close to actual open air. Before the experiments, the

190   chamber was cleaned by flushing with zero air for approximately 12 hours and

191   illuminated with sunlight, to remove residues that could influence the experiments.

192   H_2O_2 (1 mL, 30%), together with the vehicle emission, was injected into the chamber

193   to generate OH exposure. After the injection, the experiments were conducted from

194   approximately 13:00 to 17:00 local time under sunshine, with the relative humidity kept

195   around 50%. The global solar radiation when the tests were carried out was

196   approximately 318 W m^{-2}. After 3.5 h of ageing, the particles in the chamber were

197   collected onto mesh TEM grids using the impactor. The collection time for each sample

198   was 120 s. The schematic diagram of the experimental system is presented in Figure

199   S1b.

200

201   **2.3 TEM/EDX and scanning transmission electron microscopy (STEM) analyses**

202   The particles in the samples were examined using a Tecnai G2 F30 field emission

203   high-resolution transmission electron microscope (FE-HRTEM). This microscope is

204   also equipped with an Oxford EDX and a STEM unit with a high-angle annular dark-

205   field detector (HAADF). The EDX can detect elements with the atom number larger

206   than 5 (B) in a single particle. The HAADF can detect the distribution of a certain

207   element by mapping the distribution of the element in a particle. The TEM was operated

208   with the acceleration voltage of 300 kV. EDX spectra were firstly collected for 20 live

209   seconds to minimize the influence of radiation exposure and potential beam damage

210   and then for 90 live seconds for a range of possible elements. Copper was excluded

211   from the analysis because of interference from the TEM grids which are made of copper.

212   To ensure the representativeness of the analyzed particles, more than 150 particles

213   from at least 3 random areas were analyzed from the center and periphery of the

214 sampling spot on each grid. All individual particles larger than 50 nm in the selected

215 areas were analyzed. The TEM images were digitized using an automated fringe image

216 processing system to project the surface areas of the particles. The equivalent spherical

217 diameter of a particle was calculated from its projected area, expressed as the square

218 root of 4 A/π, where A is the projected area.

3. Results

3.1. Particle morphology, elemental composition and size

221   A total of 2880 particles were analyzed from the GDI-engine vehicles. Most of the

222 particles were in the sub-micrometer size range. Based on morphology and elemental

223 composition of the particles, the majority of them were identified as soot, organic and

224 Ca-rich particles, a smaller amount was identified as S-rich or metal-rich particles (Fig.

225 1). The method of particle classification is similar to that adopted by Okada et al. (2005)

226 and Xing et al. (2019). In the following description, "X-rich" means that the element

227 "X" occupies the largest proportion in the element composition of the particles. Figure

228 2 illustrates the number-size distributions of the relative concentration (dN/dlogD) of

229 primary particles from the GDI-engine vehicle, where N is the relative number fraction

230 and D is the equivalent diameter. The particles were in the range of 60–2500 nm and

231 displayed a bimodal distribution, with one mode in the 140–240 nm range, and another

232 in the 800–900 nm range. Particles smaller than 250 nm were largely underestimated

233 because of the loss during the particle collection. Therefore, there should have been

234 more particles in the smaller mode range than shown in Figure 2.

235   It should be noted that organic particles were mainly composed of C and O

236 elements, and contained a small amount of inorganic elements Ca, P, S and Zn.

237   Elemental mapping of the organic particles exhibited the presence of Ca, P, S and Zn in

238   some of the particles, showing the mixture state of organic and inorganic materials (Fig.

239   1f). It has been reported that such particles could be related to the combustion of fuels

240   or lubrication oil (Rönkkö et al. 2013). In addition to these primary organic particles,

241   the GDI-engine vehicle emitted precursor gases, which produced secondary organic

242   particles via gas-phase reactions, and multiphase and heterogeneous processes on the

243   primary particles. A group of spherical particles were found in the environmental

244   chamber (Fig. 1g). These particles became semi-transparent or transparent to an

245   electron beam, which is characteristic of organic materials, liquid water, or their

246   evaporation residues either mixed or not mixed with electron absorptive materials. We

247   regard these particles as secondary organic particles because the humidity in the

248   chamber during the experiment was kept much below saturation (relative humidity

249   around 50%). Therefore, these particles were expected to mainly consist of secondary

250   organic materials, which should have been produced via gas phase reactions or on the

251   surface of pre-existing particles (Hu et al. 2016). No other elements, except C and O,

252   were identified in these particles, which is consistent with the above inference. Similar

253   particles were also encountered in other environmental chamber experiments studying

254   emissions from light-duty gasoline vehicles (Jathar et al. 2014).

255

256   **3.2 Number fractions of particles**

257   Figure 3 illustrates the numbers of accumulation mode particles emitted by

258   burning one kilogram of fuel during the cold start and hot start driving cycles. PM

259   emissions at the start-up stage under both cold and hot start states were higher than the

260 emissions under the states when the engine was fully warmed and the vehicle operation

261 was stabilized. The PM emission was the highest under the hot stabilized running state

262 (2.3×10^{10} particles (kg fuel)$^{-1}$), followed by those under the hot start (1.2×10^{10} particles

263 (kg fuel)$^{-1}$), cold start (7.1×10^{9} particles (kg fuel)$^{-1}$), and acceleration running states

264 (2.9×10^{9} particles (kg fuel)$^{-1}$). The emission was the lowest under the idle running state

265 (7.4×10^{8} particles (kg fuel)$^{-1}$) (Fig. S2).

266 Under all the running states, we found similarities in particles morphologies and

267 types. However, the proportions of particle types differed considerably (Fig. S3). The

268 fractions of organic particles were high under hot stabilized and hot start states. Soot

269 particles were abundant under cold start and acceleration states. A relatively higher

270 fraction of Ca-rich particles was found under idle state, compared to those under other

271 running states.

272 We estimated the number of different type particles in the emission under the

273 running states by burning one kilogram of fuel (Fig. 4). Organic particles in the

274 emission under the hot stabilized running state (2.3×10^{9} particles (kg fuel)$^{-1}$) and the

275 hot start running state (3.6×10^{8} particles (kg fuel)$^{-1}$) were higher than in the emission

276 under other running states. The number of soot particles were higher under the hot

277 stabilized running state (1.7×10^{9} particles (kg fuel)$^{-1}$) and the cold start state (5.9×10^{8}

278 particles (kg fuel)$^{-1}$) than those under other running states. Under the idle state, the

279 relative proportion of Ca-rich particles was the highest, although their absolute number

280 was low (1.4×10^{9} particles (kg fuel)$^{-1}$).

281 Under the cold start state, a significant proportion of the emitted particles were

282 soot particles. This can be attributed to the incomplete vaporization of fuel droplets in

283 the combustion cylinder (Chen et al. 2017). Under the hot start state and the hot

284 stabilized running state, organic particles were predominant. Under these two running

285 states, the engine temperature was high, which enabled the fuel to evaporate and mix

286 with the air easily. With the temperature in the cylinders increasing, the rate of particle

287 oxidation increased, which could cause an increase of organic particles in the emission

288 (Fu et al. 2014). Under the idle state, the fuel consumption was much lower than that

289 under the other running states, which results in the relative contribution of lubricant oil

290 to particles in the emission being higher. The high Ca content in the lubricant oil led to

291 a higher Ca-rich particle emission under this running state. Under the acceleration state,

292 the predominant particle types included soot, organic, and Ca-rich particles. As the

293 acceleration running required a high vehicular speed and engine load, the emissions

294 contained more soot particles than those under other running states.

295 **3.3. Aged particles in the environmental chamber**

296 Secondary organic particles, some soot particles, Ca-rich particles, and primary

297 organic particles were detected in the environmental chamber (Fig. 5). After the ageing

298 process, many soot particles changed into core-shell structures and became coated with

299 secondary species (Figs. 5b and 5c). The morphology and compositions of Ca-rich

300 particles and organic particles (Figs. 5e and 5g) changed, and the aged ones had a higher

301 sulfur (S) content in comparison with the fresh ones (Figs. 5A and B). Approximately

302 80% of the soot particles were present in core-shell structures and coated with

303 secondary species after the 3.5-hour ageing. In contrast, before the ageing, the particles

304 with a core-shell structure were only about 10% of the total. The mean diameter of the

305   soot particles after ageing was around 0.49 µm, which was much smaller than that

306   before the ageing (0.65 µm), indicating the shrinkage of some particles during the

307   ageing (Fig. 5b).

308   **4. Discussion**

309   **4.1. Contribution of GDI-engine vehicle emissions to urban air pollution**

310   Our investigation shows that the GDI-engine vehicle emitted a large amount of

311   soot, organic particles, and Ca-rich particles. Considering the large fraction of vehicles

312   equipped with GDI engines in megacities like Beijing, this indicates a possible

313   substantial contribution of GDI-engine vehicles to urban air pollution. Moreover,

314   organic particles occupied the majority of the particles emitted under hot stabilized

315   running and hot start states. The hot stabilized running state is the most frequent running

316   condition of vehicles, whereas the hot start state is the most frequent condition in

317   congested traffic. This suggests that a substantial number of organic compounds in the

318   air pollution of populated cities might be directly related to vehicle emissions.

319   Organic particles and soot particles in ambient air are emitted from a range of

320   sources including fossil fuels, biomass burning and urban waste burning (Kanakidou et

321   al. 2005). Table 1 shows the major characteristics of particles in the emissions from

322   different sources. For instance, there is a higher fraction of soot particles and a lower

323   fraction of organic particles in the emissions of GDI-engine vehicles compared to PFI-

324   engine vehicles. Organic particles in emissions from gasoline vehicles are usually

325   enriched in Ca, S and P (Xing et al. 2017, Liati et al. 2018). In comparison, emissions

326   from biomass/wood burning are usually dominated by organic particles, which account

327 for more than 50% of the total amount of particles (Liu et al. 2017). Furthermore,

328 organic particles from biomass/wood burning usually show elevated K content, and

329 thus, this element is frequently used as an indicator for biomass/wood burning organic

330 particles (e.g. Niu et al. 2016). Observations of primary particles directly from coal

331 burning have also demonstrated a predominance of organic particles, soot particles, S-

332 rich particles and mineral particles (Zhang et al. 2018, Wang et al. 2019). Both biomass

333 burning and coal combustion can produce organic particles and almost all the emitted

334 particles contain a certain amount of Si in addition to C and O. Table 1 also shows the

335 elemental concentrations in the organic particles in the emissions from different types

336 of sources. Since the concentrations of minor elements in the organic particles are

337 highly dependent on the sources, they could be used for unambiguous source

338 identification of individual particles in the atmosphere.

339 The present data also permit the compilation of a rough inventory of particle

340 categories and amounts emitted from GDI-engine vehicles under various running

341 conditions (Fig. 4). Combined with statistics on the number of vehicles with GDI

342 engines, the running time and the running conditions on roads within a certain area, it

343 is possible to make an approximate estimate of the amounts of primary particles emitted

344 from GDI-engine vehicles. Such estimate is the basis for accurate source apportioning

345 of particles from vehicles, and it will be very beneficial for studies on the anthropogenic

346 sources of primary particles in urban air. These data could be brought together to better

347 understand the sources of air pollutants in the Beijing megacity and to improve the

348 capability of developing cost-effective mitigation measures.

4.2 Rapid ageing of primary particles in Beijing

349

350   The results of chamber experiments indicate that sulfate and secondary organic

351 aerosol (SOA) form on the surface of soot, Ca-rich and organic particles. Moreover, the

352 atmospheric transformation of primary particles emitted by the GDI-engine vehicles

353 could occur within 3.5 hours, indicating the ageing was rapid. Peng et al. (2014) found

354 similar timescales for black carbon transformation under polluted conditions in Beijing.

355 The rapid ageing of primary particles could be caused by several factors, such as the

356 concentration of gaseous pollutants from the vehicles, strength of solar radiation,

357 relative humidity (RH), and O_3 concentration (Guo et al. 2012, Deng et al. 2017, Du et

358 al. 2018). The present experiments were conducted in the atmosphere with relative

359 humidity of approximately 50% and solar radiation of 318 Wm^{-2}. The total hydrocarbon

360 emission (THC) from the GDI vehicles was 0.297 g km^{-1}. Repeated braking and

361 acceleration in the BDC could cause incomplete combustion and consequently high

362 THC emission. Under a high concentration of gaseous pollutants, primary particles

363 would age rapidly when exposed to solar radiation. Consequently, secondary species

364 including SOA and sulfate were produced on or condensed onto the particles, leading

365 to the coating. Guo et al., (2014) also showed that secondary photochemical growth of

366 fine aerosols during the initial stage of haze development could be attributed to highly

367 elevated levels of gaseous pollutants.

368   Previous studies demonstrated that inorganic salts, such as sulfate, catalyze

369 carbonyl heterogeneous reactions, and consequently, lead to SOA production (Jang et

370 al. 2002, Jang et al. 2004). Our results showed that sulfate formed on the surface of soot,

Ca-rich and organic particles. These aged primary particles favored the formation of

secondary aerosols by providing reaction sites and reaction catalysts. Moreover,

Mauldin et al. (2012) reported that the VOCs oxidation products could react with SO_2

to rapidly produce sulfate. Thus, the rapid ageing of primary particles could also be

attributable to the acid-catalyzed mechanism. As the major source of pollutants in urban

air, the GDI-engine vehicles supply both primary particles and precursor gaseous

species, and the rapid ageing of the particles under certain conditions is very likely the

major driving force for the elevation of urban air pollution.

4.3 Implications and perspectives

We highlight the considerable potential contribution of GDI-engine vehicles to

both primary and secondary organic aerosols. Organic aerosols (OA) play an important

role in the Earth's radiation balance not only for its absorption and scattering of solar

radiation but also because they can alter the microphysical properties of clouds (Scott

et al. 2014). Particle size, shape, mixing state and composition affect their light

scatterings and absorption cross sections, and cloud condensation nuclei activity

(Jacobson 2001). Recent measurements indicate that most OA exists as an internal

mixture with other aerosols, and the distribution of this mixture depends on the

formation mechanism of OA (Zhu et al. 2017). However, some atmospheric models still

present the particle population as an external mixture, particularly because the

formation of OA is associated with complex and not fully understood mechanisms (Lin

et al. 2014). Using external mixture of the aerosols in models will cause the reduced

direct effect because of the decrease in total aerosol surface area and the increase of

393   absorption efficiency (Lin et al. 2014).

394   Our results showed that primary organic aerosols (POA) emitted by GDI-engine

395   vehicles could acquire OA and sulfate coatings rapidly, within a few hours, and increase

396   a sizable fraction of total ambient aerosols existing as internal mixtures. In addition, the

397   fast ageing further caused the increase of aged POA in the total OA, consequently,

398   largely modified the properties of the particles such as their optical properties.

399   Structures and compositions are critical to the ability of aerosol particles to absorb and

400   reflect solar radiation (Li et al. 2011). The results of the experiments in the chamber

401   showed that most of the aged POA had a core-shell structure, whereas most of the

402   secondary organic aerosols (SOA) produced by gas-phase reactions had a uniform

403   structure. However, studies on the optical properties of OA have been mainly focused

404   on SOA, and only a few studies dealt with POA. Our results indicate the possible

405   substantial contribution of emissions from the GDI-engine vehicles to POA, especially

406   in traffic congestion. For a better understanding of the roles that traffic emissions play

407   in urban air pollution, further segregation of the aerosol particles such as POA and SOA

408   in model and observation studies is inevitable.

409   **5. Conclusions**

410   1. Five types of individual particles emitted by the GDI-engine vehicles were

411   identified, including soot, organic, Ca-rich, S-rich, and metal-rich particles. Among

412   them, soot, organic, and Ca-rich particles were predominant. The particles emitted

413   from GDI-engine vehicles displayed a bimodal size distribution.

414   2. The concentrations of the particles under the various running conditions were

415   different. The emission (per unit fuel burned) under the cold start condition was

416   higher than that under hot start condition.

417 3. Large amounts of organic particles were emitted during hot stabilized and hot start

418   states. Under cold start and acceleration states, the emissions were enriched in soot

419   particles. Under idle state, a relatively higher number of Ca-rich particles was

420   emitted, although the absolute number was low.

421 4. After ageing in the environmental chamber, the structure of the soot particles

422   changed into a core-shell structure, and the particles were coated with condensed

423   secondary organic material. Ca-rich particles and organic particles also were

424   modified, and their content of sulfur increased after ageing.

425 5. Ageing of the emitted particles occurred rapidly, within hours. Such rapid ageing

426   could be attributable to an acid-catalyzed mechanism and to the high initial

427   concentrations of gaseous pollutants emitted by the GDI-engine gasoline.

428

Data availability

430   All data presented in this paper are available upon request. Please contact the

431 corresponding author (shaoL@cumtb.edu.cn).

Author contribution

433   LS designed this study; JX performed the experiments. JX, LS, DZ summarized

434 the data and wrote the paper. WZ, JP, WW, SS, MH supported the experiments and

435 commented the paper.

Competing interests

The authors declare that they have no conflict of interest.

Acknowledgements

This work was supported by Projects of International Cooperation and Exchanges NSFC (Grant No. 41571130031). The data analysis was partly supported by Science and Technology Project Founded by the Education Department of Jiangxi Province (No. GJJ180226), Yue Qi Scholar Fund of China University of Mining and Technology (Beijing), and a Grant-in-Aid for Scientific Research (B) (No.16H02942) from the JSPS.

References

Adachi, K., and Buseck, P. R.: Changes in shape and composition of sea-salt particles upon aging in an urban atmosphere, Atmos. Environ., 100, 1-9, http://dio.org/10.1016/j.atmosenv.2014.10.036, 2015.

Alves, C. A., Lopes, D. J., Calvo, A. I., Evtyugina, M., Rocha, S., and Nunes, T.: Emissions from light-duty diesel and gasoline in-use vehicles measured on chassis dynamometer test cycles, Aerosol Air Qual. Res., 15(1), 99-116, http://dio.org/10.4209/aaqr.2014.01.0006, 2015.

Baral, B., Raine, R., and Miskelly, G.: Effect of engine operating conditions on spark-ignition engine PAH emissions, SAE Technical Paper 2011-01-1161, http://dio.org/10.4271/2011-01-1161, 2011.

Bond, T. C., Doherty, S. J., Fahey, D. W., Forster, P. M., Berntsen, T., DeAngelo, B. J., Flanner, M. G., Ghan, S., Kärcher, B., Koch, D., Kinne, S., Kondo, Y., Quinn, P. K., Sarofim, M. C., Schultz, M. G., Schulz, M., Venkataraman, C., Zhang, H., Zhang, S., Bellouin, N., Guttikunda, S. K., Hopke, P. K., Jacobson, M. Z., Kaiser, J. W., Klimont, Z., Lohmann, U., Schwarz, J. P., Shindell, D., Storelvmo, T., Warren, S. G., and Zender, C. S.: Bounding the role of black carbon in the climate system: A scientific assessment, J. Geophys. Res.-Atmos., 118(11), 5380-5552, http://dio.org/10.1002/jgrd.50171, 2013.

Chart-asa, C., and Gibson, J. M.: Health impact assessment of traffic-related air pollution at the urban project scale: Influence of variability and uncertainty, Sci. Total Environ., 506-507, 409-421, http://dio.org/10.1016/j.scitotenv.2014.11.020, 2015.

Chen, Z., Chen, D., Xie, X., Cai, J., Zhuang, Y., Cheng, N., He, B., and Gao, B.: Spatial self-aggregation effects and national division of city-level $PM_{2.5}$ concentrations in China based on spatio-temporal clustering, J. Clean. Prod., 207, 875-881, http://dio.org/10.1016/j.jclepro.2018.10.080, 2019.

Chen, L., Liang, Z., Zhang, X., and Shuai, S.: Characterizing particulate matter emissions from GDI and PFI vehicles under transient and cold start conditions, Fuel, 189, 131-140,

469 http://dio.org/10.1016/j.fuel.2016.10.055, 2017.

470 Chen, L., and Stone, R.: Measurement of enthalpies of vaporization of isooctane and ethanol blends and
471   their effects on PM emissions from a GDI engine, Energ. Fuel, 25(3), 1254-1259,
472   http://dio.org/10.1021/ef1015796, 2011.

473 Deng, W., Hu, Q., Liu, T., Wang, X., Zhang, Y., Song, W., Sun, Y., Bi, X., Yu, J., Yang, W., Huang, X.,
474   Zhang, Z., Huang, Z., He, Q., Mellouki, A., and George, C.: Primary particulate emissions and
475   secondary organic aerosol (SOA) formation from idling diesel vehicle exhaust in China, Sci. Total
476   Environ., 593-594, 462-469, http://dio.org/10.1016/j.scitotenv.2017.03.088, 2017.

477 Du, Z., Hu, M., Peng, J., Zhang, W., Zheng, J., Gu, F., Qin, Y., Yang, Y., Li, M., Wu, Y., Shao, M., and
478   Shuai, S.: Comparison of primary aerosol emission and secondary aerosol formation from gasoline
479   direct injection and port fuel injection vehicles, Atmos. Chem. Phys., 18(12), 9011-9023,
480   http://dio.org/10.5194/acp-18-9011-2018, 2018.

481 Fu, H., Wang, Y., Li, X., and Shuai, S.: Impacts of cold-start and gasoline RON on particulate emission
482   from vehicles powered by GDI and PFI engines, SAE Technical Paper 2014-01-2836, http://dio.org/
483   10.4271/2014-01-2836, 2014.

484 Giechaskiel, B., Maricq, M., Ntziachristos, L., Dardiotis, C., Wang, X., Axmann, H., Bergmann, A., and
485   Schindler, W.: Review of motor vehicle particulate emissions sampling and measurement: From
486   smoke and filter mass to particle number, J. Aerosol Sci., 67, 48-86,
487   http://dio.org/10.1016/j.jaerosci.2013.09.003, 2014.

488 Guo, S., Hu, M., Guo, Q., Zhang, X., Zheng, M., Zheng, J., Chang, C. C., Schauer, J. J., and Zhang, R.:
489   Primary sources and secondary formation of organic aerosols in Beijing, China, Environ. Sci.
490   Technol., 18(46), 9846 – 9853, 2012.

491 Hedge, M., Weber, P., Gingrich, J., Alger, T., and Khalek, I. A.: Effect of EGR on Particle Emissions
492   from a GDI Engine, SAE Int. J. Engines, 4(1), 650- 666, http://dio.org/10.4271/2011-01-0636, 2011.

493 Hu, W., Niu, H., Zhang, D., Wu, Z., Chen, C., Wu, Y., Shang, D., and Hu, M.: Insights into a dust event
494   transported through Beijing in spring 2012: Morphology, chemical composition and impact on
495   surface aerosols, Sci. Total Environ., 565, 287-298, http://dio.org/10.1016/j.scitotenv.2016.04.175,
496   2016.

497 Huang, R., Zhang, Y., Bozzetti, C., Ho, K., Cao, J., Han, Y., Daellenbach, K. R., Slowik, J. G., Platt, S.
498   M., Canonaco, F., Zotter, P., Wolf, R., Pieber, S. M., Bruns, E. A., Crippa, M., Ciarelli, G.,
499   Piazzalunga, A., Schwikowski, M., Abbaszade, G., Schnelle-Kreis, J., Zimmermann, R., An, Z.,
500   Szidat, S., Baltensperger, U., Haddad, I. E., and Prévôt, A. S. H.: High secondary aerosol
501   contribution to particulate pollution during haze events in China, Nature, 514(7521), 218-222,
502   http://dio.org/10.1038/nature13774, 2014.

503 Jacobson, M. Z.: Strong radiative heating due to the mixing state of black carbon in atmospheric aerosols,
504   Nature, 409(6821), 695-697, http://dio.org/10.1038/35055518, 2001.

505 Jang, M. S., Czoschke, N. M., Lee, S., and Kamens, R. M.: Heterogeneous atmospheric aerosol
506   production by acid-catalyzed particle-phase reactions, Science, 298(5594), 814-817,
507   http://dio.org/10.1126/science.1075798, 2002.

508 Jang, M., Czoschke, N. M., and Northcross, A. L.: Atmospheric organic aerosol production by
509   heterogeneous acid-catalyzed reactions, Chemphyschem, 5(11), 1647-1661,
510   http://dio.org/10.1002/cphc.200301077, 2004.

511 Jathar, S. H., Gordon, T. D., Hennigan, C. J., Pye, H. O. T., Pouliot, G., Adams, P. J., Donahue, N. M.,
512   and Robinson, A. L.: Unspeciated organic emissions from combustion sources and their influence

513   on the secondary organic aerosol budget in the United States, P. Natl. Acad. Sci. USA, 111(29),
514   10473-10478, http://dio.org/10.1073/pnas.1323740111, 2014.
515 Kanakidou, M., Seinfeld, J. H., Pandis, S. N., Barnes, I., Dentener, F. J., Facchini, M. C., Van Dingenen,
516   R., Ervens, B., Nenes, A., Nielsen, C. J., Swietlicki, E., Putaud, J. P., Balkanski, Y., Fuzzi, S., Horth,
517   J., Moortgat, G. K., Winterhalter, R., Myhre, C., Tsigaridis, K., Vignati, E., Stephanou, E. G., and
518   Wilson, J.: Organic aerosol and global climate modelling: A review, Atmos. Chem. Phys., 5, 1053-
519   1123, http://dio.org/10.5194/acp-5-1053-2005, 2005.
520 Khalek, I. A., Bougher, T., and Jetter, J. J.: Particle Emissions from a 2009 gasoline direct injection
521   engine using different commercially available fuels, SAE Int. J. Fuels Lubr., 3(2), 623- 637,
522   http://dio.org/10.4271/2010-01-2117, 2010.
523 Li, W., Li, P., Sun, G., Zhou, S., Yuan, Q., and Wang, W.: Cloud residues and interstitial aerosols from
524   non-precipitating clouds over an industrial and urban area in northern China, Atmos. Environ.,
525   45(15), 2488-2495, http://dio.org/10.1016/j.atmosenv.2011.02.044, 2011.
526 Li, W., and Shao, L.: Transmission electron microscopy study of aerosol particles from the brown hazes
527   in northern china, J. Geophys. Res.-Atmos., http://dio.org/D09302, 2009.
528 Liati, A., Schreiber, D., Dasilva, Y. A. R., and Eggenschwiler, P. D.: Ultrafine particle emissions from
529   modern gasoline and diesel vehicles: An electron microscopic perspective, Environ. Pollut., 239,
530   661-669, http://dio.org/10.1016/j.envpol.2018.04.081, 2018.
531 Lin, G., Penner, J. E., Flanner, M. G., Sillman, S., Xu, L., and Zhou, C.: Radiative forcing of organic
532   aerosol in the atmosphere and on snow: Effects of SOA and brown carbon, J. Geophys. Res.-Atmos.,
533   119(12), 7453-7476, http://dio.org/10.1002/2013JD021186, 2014.
534 Liu, L., Kong, S., Zhang, Y., Wang, Y., Xu, L., Yan, Q., Lingaswamy, A. P., Shi, Z., Lv, S., Niu, H.,
535   Shao, L., Hu, M., Zhang, D., Chen, J., Zhang, X., and Li, W.: Morphology, composition, and mixing
536   state of primary particles from combustion sources - crop residue, wood, and solid waste, Sci. Rep.-
537   UK, http://dio.org/10.1038/s41598-017-05357-2, 2017.
538 Luo, Y., Zhu, L., Fang, J., Zhuang, Z., Guan, C., Xia, C., Xie, X., and Huang, Z.: Size distribution,
539   chemical composition and oxidation reactivity of particulate matter from gasoline direct injection
540   (GDI) engine fueled with ethanol-gasoline fuel, Appl. Therm. Eng., 89, 647-655,
541   http://dio.org/10.1016/j.applthermaleng.2015.06.060, 2015.
542 Maricq, M. M., Szente, J., Loos, M., and Vogt, R.: Motor vehicle PM emissions measurement at LEV
543   III levels, SAE Int. J. Engines, 4(1), 597- 609, http://dio.org/10.4271/2011-01-0623, 2011.
544 Mauldin, R. L. I., Berndt, T., Sipilae, M., Paasonen, P., Petaja, T., Kim, S., Kurten, T., Stratmann, F.,
545   Kerminen, V., and Kulmala, M.: A new atmospherically relevant oxidant of sulphur dioxide, Nature,
546   488(7410), 193-196, http://dio.org/10.1038/nature11278, 2012.
547 National Bureau of Statistics of China, 2018. China Statistical Yearbook 2018, part sixteen:
548   Transportation, post and telecommunications and software industry. Available on line at:
549   http://www.stats.gov.cn/tjsj/ndsj/2018/indexch.htm, 2018.
550 Niu, H., Cheng, W., Hu, W., and Pian, W.: Characteristics of individual particles in a severe short-period
551   haze episode induced by biomass burning in Beijing, Atmos. Pollut. Res., 7(6), 1072-1081,
552   http://dio.org/10.1016/j.apr.2016.05.011, 2016.
553 Niu, H., Shao, L., and Zhang, D.: Aged status of soot particles during the passage of a weak cyclone in
554   Beijing, Atmos. Environ., 45(16), 2699-2703, http://dio.org/10.1016/j.atmosenv.2011.02.056, 2011.
555 Okada, K., Qin, Y., and Kai, K.: Elemental composition and mixing properties of atmospheric mineral
556   particles   collected   in   Hohhot,   China,   Atmos.   Res.,   73(1-2),   45-67,

557   http://dio.org/10.1016/j.atmosres.2004.08.001, 2005.

558   Peng, J., Hu, M., Guo, S., Du, Z., Shang, D., Zheng, J., Zheng, J., Zeng, L., Shao, M., Wu, Y., Collins,
559   D., and Zhang, R.: Ageing and hygroscopicity variation of black carbon particles in Beijing
560   measured by a quasi-atmospheric aerosol evolution study (QUALITY) chamber, Atmos. Chem.
561   Phys., 17(17), 10333-10348, http://dio.org/10.5194/acp-17-10333-2017, 2017.

562   Petzold, A., Marsh, R., Johnson, M., Miller, M., Sevcenco, Y., Delhaye, D., Ibrahim, A., Williams, P.,
563   Bauer, H., Crayford, A., Bachalo, W. D., and Raper, D.: Evaluation of methods for measuring
564   particulate matter emissions from gas turbines, Environ. Sci. Technol., 45(8), 3562-3568, 2011.

565   Rönkkö, T., Lähde, T., Heikkilä, J., Pirjola, L., Bauschke, U., Arnold, F., Schlager, H., Rothe, D., Yli-
566   Ojanperä, J., and Keskinen, J.: Effects of gaseous sulphuric acid on diesel exhaust nanoparticle
567   formation and characteristics, Environ. Sci. Technol., 47(20), 11882-11889,
568   http://dio.org/10.1021/es402354y, 2013.

569   Scott, C. E., Rap, A., Spracklen, D. V., Forster, P. M., Carslaw, K. S., Mann, G. W., Pringle, K. J.,
570   Kivekas, N., Kulmala, M., Lihavainen, H., and Tunved, P.: The direct and indirect radiative effects
571   of biogenic secondary organic aerosol, Atmos. Chem. Phys., 14(1), 447-470,
572   http://dio.org/10.5194/acp-14-447-2014, 2014.

573   Shao, L., Hu, Y., Fan, J., Wang, J., Wang, J., and Ma, J.: Physicochemical characteristics of aerosol
574   particles in the Tibetan Plateau: Insights from TEM-EDX analysis, J. Nanosci. Nanotechno., 17(9),
575   6899-6908, http://dio.org/10.1166/jnn.2017.14472, 2017.

576   Shao, L., Hu, Y., Shen, R., Schäfer, K., Wang, J., Wang, J., Schnelle-Kreis, J., Zimmermann, R., BéruBé,
577   K., and Suppan, P.: Seasonal variation of particle-induced oxidative potential of airborne particulate
578   matter in Beijing, Sci. Total Environ., 579, 1152-1160,
579   http://dio.org/10.1016/j.scitotenv.2016.11.094, 2017.

580   Shi, Z., Vu, T., Kotthaus, S., Harrison, R. M., Grimmond, S., Yue, S., Zhu, T., Lee, J., Han, Y., Demuzere,
581   M., Dunmore, R. E., Ren, L., Liu, D., Wang, Y., Wild, O., Allan, J., Acton, W. J., Barlow, J., Barratt,
582   B., Beddows, D., Bloss, W. J., Calzolai, G., Carruthers, D., Carslaw, D. C., Chan, Q., Chatzidiakou,
583   L., Chen, Y., Crilley, L., Coe, H., Dai, T., Doherty, R., Duan, F., Fu, P., Ge, B., Ge, M., Guan, D.,
584   Hamilton, J. F., He, K., Heal, M., Heard, D., Hewitt, C. N., Hollaway, M., Hu, M., Ji, D., Jiang, X.,
585   Jones, R., Kalberer, M., Kelly, F. J., Kramer, L., Langford, B., Lin, C., Lewis, A. C., Li, J., Li, W.,
586   Liu, H., Liu, J., Loh, M., Lu, K., Lucarelli, F., Mann, G., McFiggans, G., Miller, M. R., Mills, G.,
587   Monk, P., Nemitz, E., O'Connor, F., Ouyang, B., Palmer, P. I., Percival, C., Popoola, O., Reeves,
588   C., Rickard, A. R., Shao, L., Shi, G., Spracklen, D., Stevenson, D., Sun, Y., Sun, Z., Tao, S., Tong,
589   S., Wang, Q., Wang, W., Wang, X., Wang, X., Wang, Z., Wei, L., Whalley, L., Wu, X., Wu, Z.,
590   Xie, P., Yang, F., Zhang, Q., Zhang, Y., Zhang, Y., and Zheng, M.: Introduction to the special issue
591   "In-depth study of air pollution sources and processes within Beijing and its surrounding region
592   (APHH-Beijing)", Atmos. Chem. Phys., 19(11), 7519-7546, http://dio.org/10.5194/acp-19-7519-
593   2019, 2019.

594   Suarez-Bertoa, R., Zardini, A. A., Platt, S. M., Hellebust, S., Pieber, S. M., El Haddad, I., Temime-
595   Roussel, B., Baltensperger, U., Marchand, N., Prévôt, A. S. H., and Astorga, C.: Primary emissions
596   and secondary organic aerosol formation from the exhaust of a flex-fuel (ethanol) vehicle, Atmos.
597   Environ., 117, 200-211, http://dio.org/10.1016/j.atmosenv.2015.07.006, 2015.

598   Szybist, J. P., Youngquist, A. D., Barone, T. L., Storey, J. M., and Moore, W. R.: Ethanol blends and
599   engine operating strategy effects on light-duty spark-ignition engine particle emissions, Energ. Fuel.,
600   25(11), 4977-4985, http://dio.org/10.1021/ef201127y, 2011.

601 Wang, G., Zhang, F., Peng, J., Duan, L., Ji, Y., Marrero-Ortiz, W., Wang, J., Li, J., Wu, C., Cao, C.,
602   Wang, Y., Zheng, J., Secrest, J., Li, Y., Wang, Y., Li, H., Li, N., and Zhang, R.: Particle acidity and
603   sulfate production during severe haze events in China cannot be reliably inferred by assuming a
604   mixture of inorganic salts, Atmos. Chem. Phys., 18(14), 10123-10132, http://dio.org/10.5194/acp-
605   18-10123-2018, 2018.
606 Wang, W., Shao, L., Li, J., Chang, L., Zhang, D., Zhang, C., and Jiang, J.: Characteristics of individual
607   particles emitted from an experimental burning chamber with coal from the lung cancer area of
608   Xuanwei, China, Aerosol Air Qual. Res., 19(2), 355-363, http://dio.org/10.4209/aaqr.2018.05.0187,
609   2019.
610 Xing, J., Shao, L., Zhang, W., Peng, J., Wang, W., Hou, C., Shuai, S., Hu, M., and Zhang, D.:
611   Morphology and composition of particles emitted from a port fuel injection gasoline vehicle under
612   real-world driving test cycles, J. Environ. Sci-China, 76, 339-348,
613   http://dio.org/10.1016/j.jes.2018.05.026, 2019.
614 Xing, J., Shao, L., Zheng, R., Peng, J., Wang, W., Guo, Q., Wang, Y., Qin, Y., Shuai, S., and Hu, M.:
615   Individual particles emitted from gasoline engines: Impact of engine types, engine loads and fuel
616   components, J. Clean. Prod., 149, 461-471, http://dio.org/10.1016/j.jclepro.2017.02.056, 2017.
617 Xing, L., Wu, J., Elser, M., Tong, S., Liu, S., Li, X., Liu, L., Cao, J., Zhou, J., El-Haddad, I., Huang, R.,
618   Ge, M., Tie, X., Prevot, A. S. H., and Li, G.: Wintertime secondary organic aerosol formation in
619   Beijing-Tianjin-Hebei (BTH): Contributions of HONO sources and heterogeneous reactions, Atmos.
620   Chem. Phys., 19(4), 2343-2359, http://dio.org/10.5194/acp-19-2343-2019, 2019.
621 Yu, L., Wang, G., Zhang, R., Zhang, L., Song, Y., Wu, B., Li, X., An, K., and Chu, J.: Characterization
622   and source apportionment of $PM_{2.5}$ in an urban environment in Beijing, Aerosol Air Qual. Res.,
623   13(2), 574-583, 2013.
624 Zhang, H., Cheng, S., Li, J., Yao, S., and Wang, X.: Investigating the aerosol mass and chemical
625   components characteristics and feedback effects on the meteorological factors in the
626   Beijing-Tianjin-Hebei region, China, Environ. Pollut., 244, 495-502,
627   http://dio.org/10.1016/j.envpol.2018.10.087, 2019.
628 Zhang, Y., Yuan, Q., Huang, D., Kong, S., Zhang, J., Wang, X., Lu, C., Shi, Z., Zhang, X., Sun, Y.,
629   Wang, Z., Shao, L., Zhu, J., and Li, W.: Direct observations of fine primary particles from residential
630   coal burning: Insights into their morphology, composition, and hygroscopicity, J. Geophys. Res.-
631   Atmos., 123(22), 12,964-12,979, http://dio.org/10.1029/2018JD028988, 2018.
632 Zhu, J., Penner, J. E., Lin, G., Zhou, C., Xu, L., and Zhuang, B.: Mechanism of SOA formation
633   determines magnitude of radiative effects, P. Natl. Acad. Sci. USA, 114(48), 12685-12690,
634   http://dio.org/10.1073/pnas.1712273114, 2017.
635 Zimmerman, N., Wang, J. M., Jeong, C., Ramos, M., Hilker, N., Healy, R. M., Sabaliauskas, K., Wallace,
636   J. S., and Evans, G. J.: Field measurements of gasoline direct injection emission factors: Spatial and
637   seasonal variability, Environ. Sci. Technol., 50(4), 2035-2043,
638   http://dio.org/10.1021/acs.est.5b04444, 2016.
639
640

Study	Source	Particle type and relative percentages	Chemical composition of organic particles
This study	GDI-engine vehicles	Organic particles (OM) (32%), Soot (32%), Ca-rich particles (26%), S-rich (5%) and metal-containing particles (4%)	OM with Ca and weak P, S, and Zn
Xing et al. (2019)	PFI-engine vehicles	OM (44%), soot (23%), Ca-rich particles (20%), S-rich (6%) and metal-containing particles (6%).	OM with Ca and weak P, S, and Zn.
Liati et al. (2018)	GDI, PFI and diesel vehicles	Soot, OM (called ash-bearing soot particles) and ash particles.	OM with Ca, S, P, Fe and minor Zn.
Liu et al. (2017)	Crop residue combustion	OM (27%), OM-K (43%), OM-soot-K (27%), soot-OM (3%).	OM particles with K content.
Liu et al. (2017)	Wood combustion	OM (16%), soot (18%), OM-K (22%), OM-soot-K (15%), soot-OM (29%).	OM particles with K content.
Wang et al. (2019)	Coal burning	OM (38%), soot (40%), S-rich particles (2%), and mineral particles (18%).	OM mainly consisted of C, O and Si.
Zhang et al. (2018)	Residential coal burning	OM (51%), OM-S (24%), soot-OM (23%), S-rich (1%), metal-rich particles (1%), mineral particles (1%).	OM contained C, O, and Si with minor amounts of S and Cl.

List of figures:
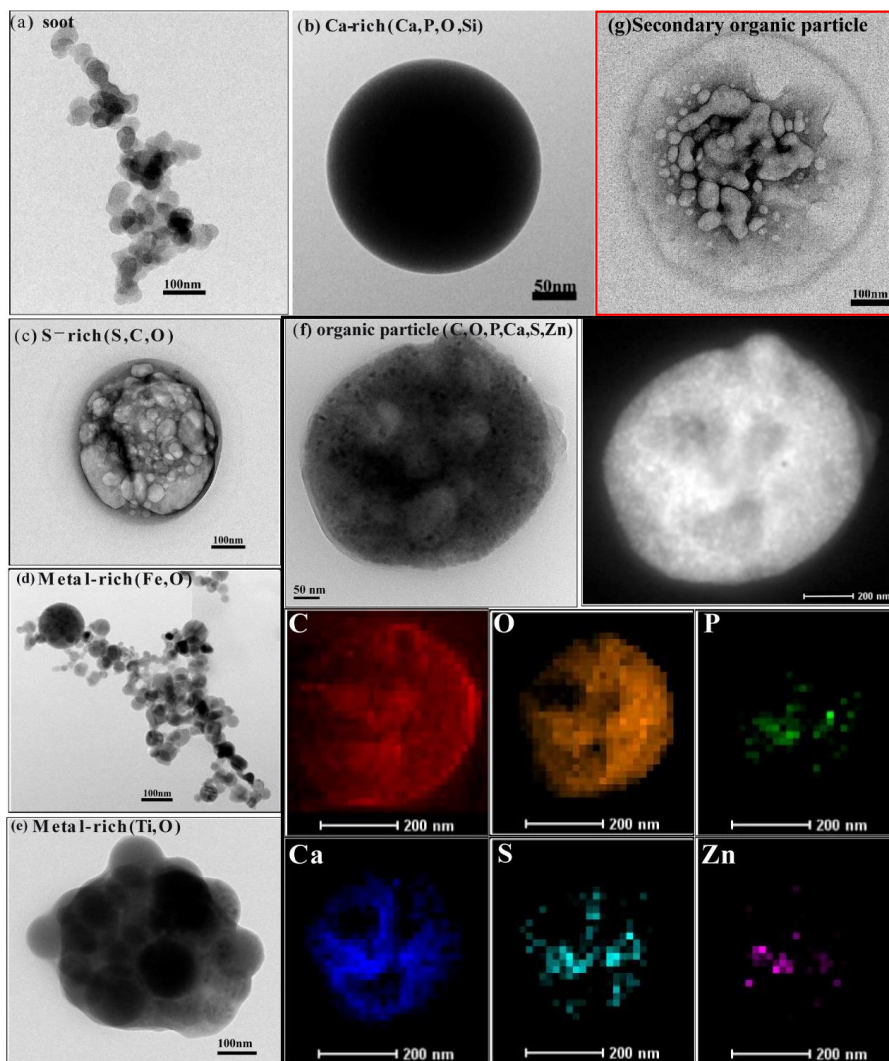
Figure 1. TEM images of the individual primary particles emitted from the GDI-engine gasoline vehicle and the secondary organic particle in the chamber after exposure to ambient sunlight for 3.5 hours. (a) soot particle; (b) Ca-rich particle; (c) S-rich particles; (d) Metal-rich particles (Fe); (e) Metal-rich particles (Ti); (f) bright-field-TEM and dark-field-TEM image of organic particles, and others are the mapping of the C, O, P, Ca, S, and Zn in the organic particle; (g) secondary organic particle in chamber.

655
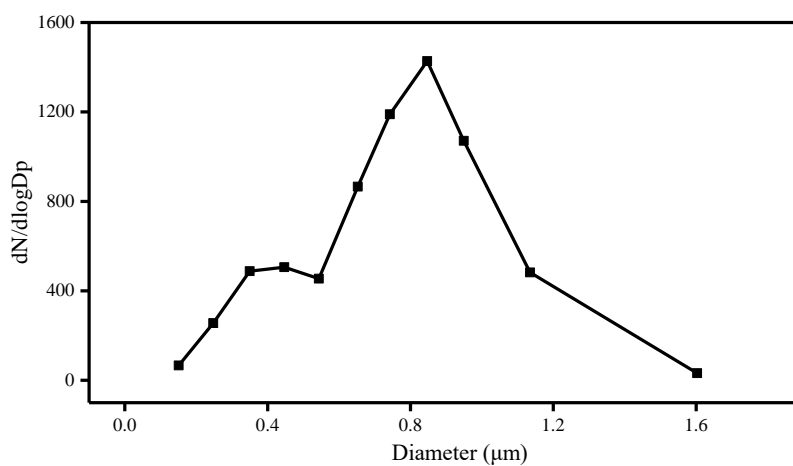
Figure 2. Size distribution of analyzed particles emitted from the GDI-engine gasoline vehicles. In total, 2880 particles were analyzed from the GDI-engine vehicles. Particles smaller than 0.25 μm should have been underestimated because of the collection efficiency of the impactor.

660

661

662   (a)
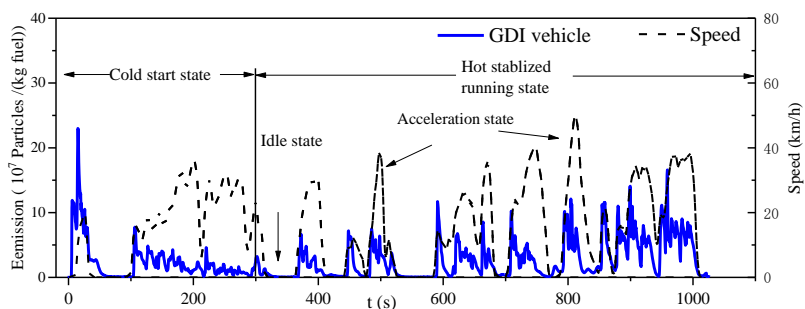
663

664   (b)
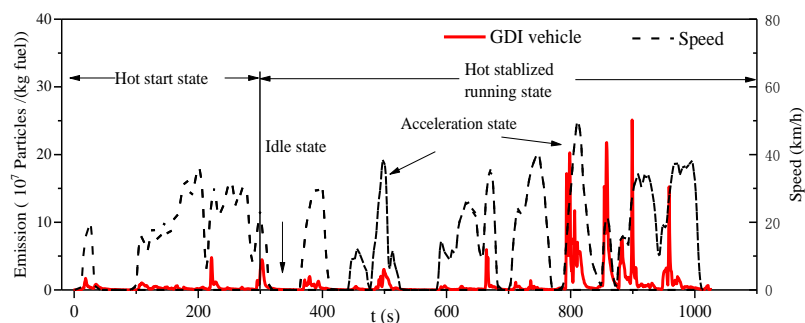
665

666   Figure 3. Particles in accumulation mode from the GDI vehicle during cold start (a) and
667   hot start (b) driving cycle. The vehicle speed is also shown for reference. Before the
668   test with cold start, the temperatures of the engine coolant and oil could not differ by
669   more than 2 °C during the soak temperature. The hot start test was conducted within 5
670   mins after the cold start test. The number concentration of particles during the tests was
671   monitored by DMS 500.

672

673

674
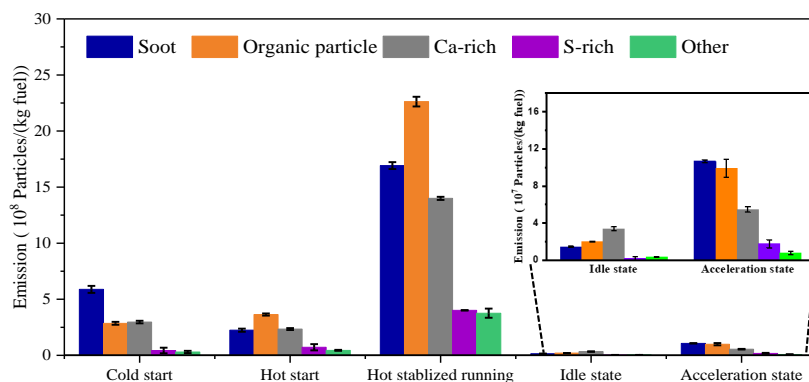
675

676   Figure 4. The number of different type particles in the emissions from the GDI vehicle

677   under the different running states by the burning of per unit of fuel, including cold start,

678   hot start, hot stabilization, idle, and acceleration states. Data presented as

679   mean ± standard deviation, N = 3.

680

681
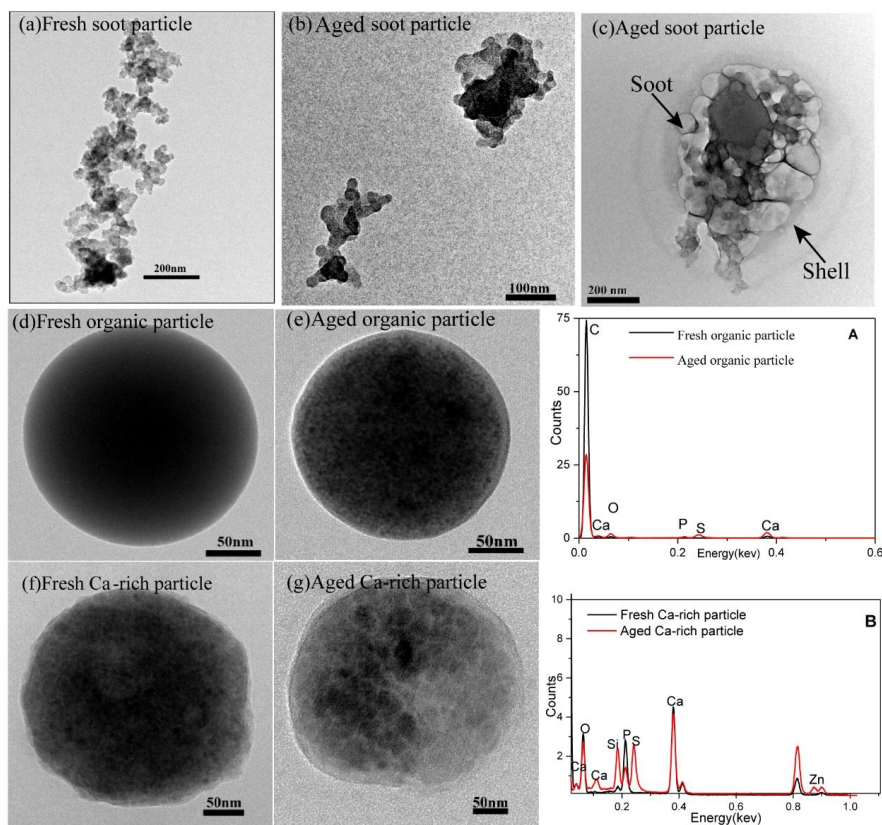
Figure 5. TEM images of particles in the chamber after exposure to ambient sunlight
for 3.5 hours. (a) Fresh soot particles; (b) Aged soot particles; (c) Aged soot particle (d)
Fresh organic particle (e) Aged organic particle (f) Fresh Ca-rich particle (g) Aged Ca-
rich particle (A) EDX spectrum for a fresh organic particle and an aged organic particle.
(B) EDX spectrum for a fresh organic particle and an aged Ca-rich particle.